Establishment of a novel asymmetric force degenerative lumbar scoliosis aging bipedal rat model

JING PENG, DAIGUI CAO, XU ZHOU, ZHIWEI LIU, XINXING WANG, ANWEI ZHANG and KAI SHEN

Department of Orthopedics, Chongqing General Hospital, Chongqing University, Chongqing 401147, P.R. China

Received January 26, 2026; Accepted July 15, 2026

DOI: 10.3892/etm.2026.13268

Abstract. The present study developed a long-term asymmetric force (AF)-induced degenerative lumbar scoliosis (DLS) model using bipedal upright rats and aimed to elucidate the role of AF in DLS pathogenesis. Sprague-Dawley rats underwent humeral head resection and tail amputation, with elevated food placement to encourage bipedal standing and feeding. The present training protocol continued for 16 weeks to establish the bipedal rat model. Subsequently, an AF-induced DLS rat model was established by implanting a nickel-titanium spring with anchor screws for 24, 36 and 48 weeks, respectively. X-ray imaging, micro-computed tomography, transmission electron microscopy, hematoxylin and eosin staining and safranin-O-fast green staining were performed. AF was associated with structural lumbar scoliosis in bipedal rats. Prolonged AF exposure reduced bone volume fraction, trabecular number, trabecular thickness, bone mineral density and tissue mineral density in the L3 lower vertebral endplate, ultimately leading to bone loss, microarchitectural deterioration, diminished mechanical strength and DLS development, although structure model index and trabecular separation remained unaffected. Prolonged asymmetric stress also caused structural damage to the medullary nerve fibers, degeneration and necrosis of intervertebral disc cartilage endplate cells, disorder of annulus fibrosus and reduction of nucleus pulposus cells. Additionally, long-term AF stimulation may have induced compensatory chondrocyte proliferation, contributing to early pathological repair processes, but appeared to reach a saturation point with extended exposure. The present study therefore successfully established a novel AF-induced DLS aging bipedal rat model, providing a basis for exploring therapeutic strategies targeting mechanical stress intervention in DLS.

Correspondence to: Dr Kai Shen, Department of Orthopedics, Chongqing General Hospital, Chongqing University, 118 Xingguang Avenue, Chongqing 401147, P.R. China
E-mail: docshen67@cqu.edu.cn

Key words: asymmetric force, degenerative lumbar scoliosis, spine, bipedal rats, micro-computed tomography

Introduction

Degenerative lumbar scoliosis (DLS) manifests as a spinal deformity marked by lateral curvature exceeding 10˚ in the coronal plane (Cobb angle), arising from structural misalignment secondary to intervertebral disc and facet joint degeneration after skeletal maturity (1). Clinical data indicates that the prevalence of adult DLS can reach 2-68%, with a mean baseline age of onset at 54.4 years, and a higher occurrence rate in women than men (2-5). This incidence rises substantially with aging populations. By 2050, the proportion of people aged 60 years and older is expected to double (6). Progressive spinal torsion and misalignment typically produce S- or C-shaped deformities, whereas vertebral displacement may compress neural structures, frequently resulting in low back pain, sensory disturbances, motor deficits and autonomic dysfunction. As a prevalent condition severely affecting middle-aged and elderly populations, DLS represents a key clinical and research focus within spinal neurosurgery (7). Although studies suggest that the etiological factors of DLS are associated with age-related spinal changes [such as intervertebral disc degeneration (IDD), facet joint imbalance and asymmetric paraspinal muscle atrophy], as well as sex, genetics and environmental influences (8-13), its core pathophysiology remains unclear. The precise biomechanical mechanisms driving disease progression particularly require further clarification (14).

Asymmetric force (AF), a key factor in spinal biomechanics, arises when external forces or internal stresses create unequal mechanical distribution across bilateral spinal structures (15). This imbalance contributes to spinal deformity progression through several mechanisms during degenerative processes. For instance, IDD reduces disc height, which destabilizes spinal segments and redistributes local stresses to produce asymmetric loading (16). Compensatory muscle imbalances on either side of the spine may further amplify AF, accelerating scoliotic deformation (17). With advances in biomechanical research in recent years, the role of AF in spinal deformity progression has gained increasing recognition (18,19). Studies have shown that AF is a key factor driving the progression of DLS (20,21). In scoliotic spines, vertebral bodies and discs on the concave side sustain disproportionately high mechanical stress, impairing vertebral growth. The vertebral endplate, derived from secondary ossification centers after ossification ceases, regulates longitudinal vertebral development (22,23).

Analyzing endplate microstructural adaptations to asymmetric loading could reveal why concave-side vertebrae exhibit growth retardation.

The establishment of animal models for scoliosis is key for investigating its pathophysiology and developing therapeutic interventions. However, current research on DLS primarily relies on clinical imaging or *in vitro* cellular biomechanical models, which fail to replicate the complex *in vivo* biomechanical environment (24,25). Existing animal models (such as spinal fusion in mice or intervertebral disc compression in rabbits) exhibit notable limitations (26). Quadrupedal locomotion results in uneven axial load distribution along the spine, rendering these models incapable of simulating human lumbar biomechanics in an upright posture (27). The majority of current models induce spinal curvature through acute surgical interventions, which contrasts with the chronic progressive nature of human DLS. Furthermore, while DLS is an age-dependent disorder, few models incorporate aged animals with long-term controlled mechanical stress interventions (28,29).

In light of the aforementioned challenges, the present study aimed to develop a bipedal upright rat model which combined bipedalization surgery with an AF system using nickel-titanium (NT) springs. The present model aims to simulate human upright biomechanics while applying controlled chronic stress, successfully inducing DLS under long-term AF conditions. This model aims to elucidate the pathophysiological mechanisms by which long-term AF accelerates the progression of DLS. The findings of the present study will aim not only contribute to a deeper understanding of DLS pathophysiology but also provide new insights and methodologies for developing clinical treatment strategies.

Materials and methods

Animals. A total of 60 Sprague-Dawley rats (4 weeks; 30 male and 30 female; SPF grade; body weight, 100-110 g) were purchased from Chengdu Dashuo Laboratory Animal Co., Ltd. (license no. 2020-0030). Rats were acclimated to standard pathogen-free housing conditions for 1 week. During this period, they had unrestricted access to water and food, while being maintained in an environment with a temperature range of 22-24˚C, humidity between 50 and 60% and a 12 h light/dark cycle. The total experimental duration was 64 weeks, consisting of 1 week of acclimation, 16 weeks of bipedal training and up to 48 weeks of postoperative observation. All procedures were approved by the Experimental Animal Ethics Committee of West China Hospital, Sichuan University (approval no. 20230412009) and were conducted in accordance with the ARRIVE 2.0 guidelines (30). The health and behavior of all animals were monitored twice daily throughout the present study. Humane endpoints for early euthanasia were predefined as follows: Weight loss >20% of peak body weight, complete anorexia for 24 h, inability to stand or move to access food and water, wound dehiscence or signs of severe infection unresponsive to treatment, and a moribund state. No animals reached these endpoints prior to their scheduled time points. All efforts were made to minimize animal suffering and to reduce the number of animals used, in accordance with the 3Rs principle.

Establishing the bipedal rat model. All rats underwent preoperative X-ray examination to exclude congenital scoliosis, following the established method for the modified bipedal rat model (27,31,32). Anesthesia was induced with 3-5% isoflurane in oxygen, resulting in loss of muscle tone within 1-3 min, and was maintained with 1-2% isoflurane throughout the surgical procedure. Placed in a supine position, the lower limbs and heads of the rats were secured. Bilateral axillary incisions were performed, followed by the careful removal of the humeral heads and all adjoining muscles and nerves. The axillary arteries and veins were then isolated, ligated and the incision sites were sutured. Surgical sutures were also applied at the base of the tail of each rat, which was subsequently amputated at the distal end of the suture site using surgical scissors. Additional sutures were administered to the stump to control bleeding. Post-surgery, the bipedal rats received meticulous care, and their feeding arrangements were gradually adjusted, with food placement raised to encourage upright standing and eating. This training regime lasted for 16 weeks, ensuring the rats fully adapted to upright living and achieved skeletal maturity (typically reached at 12 weeks of age).

Establishment of the AF-induced DLS rat model. After the 16-week bipedalization period, rats were confirmed scoliosis-free by X-ray and then randomly assigned to one of six groups using a random number table: Control (24 weeks), control (36 weeks), control (48 weeks), AF (24 weeks), AF (36 weeks) and AF (48 weeks), with 10 rats in each group. The sample size was determined using G*Power 3.1.9.7 software (Franz Faul, Universitat Kiel), setting the effect size to 0.25, α error probability to 0.05 and power (1-β error probability) to 0.80, and a total sample size of 60, which resulted in 10 rats per group, to achieve a power of 0.8. An AF-induced DLS rat model was established by implanting an NT spring combined with anchor screws (29). Rats in the AF group underwent a 12 h fast and water deprivation prior to surgery. To prevent infection, penicillin (100,000 U/kg) was administered intraperitoneally before the procedure. After successful anesthesia, the rats were placed on the operating table. The L1-L6 segment was located and marked for a midline incision. Following routine disinfection and draping, a longitudinal incision was made, and microsurgical instruments were used to expose the bony structure of the right spine. The midpoint of the transverse process roots of L1 and L6 was selected for anchor screw placement. A 25-gauge needle was used to drill obliquely into the vertebral bone, with an inward inclination of ~30-40˚ and a depth of ~5 mm. An intraoperative X-ray examination was performed to confirm the correct position of the positioning needle. After confirming the correct position of the positioning needle, the L1 and L6 positioning needles were slowly pulled out, and self-tapping titanium alloy anchor screws (1.4x6.0 mm) were placed using the micro implants orthodontic temporary anchorage device system. The ends of the NT coil springs (CAS1212, medium force, 0.012 inch and 12 mm) were then fixed to the tails of the L1 and L6 anchor screws using non-absorbable sutures. During fixation, attention was paid to adjusting the spring length so that after the spring and anchor screws on both sides were fixed, the spring was passively stretched, thus applying a certain tensile force to the right side of L1-L6, forming an AF on the lumbar spine.

After completing the implantation procedure, the area was thoroughly rinsed with normal saline, bleeding was stopped, and the incision was sutured layer by layer. The groups then continued standardized breeding for 24, 36 and 48 weeks. Penicillin (100,000 U/kg) was injected intraperitoneally once a day for 3 days postoperatively to prevent wound infection, and the incision was disinfected with iodine twice a day. The sutures were removed 3 days after surgery.

X-ray imaging techniques. Using X-ray imaging techniques, the occurrence of DLS was confirmed. After anesthetizing the rats, they were placed on an X-ray examination table, and the primary position and lateral position of the lumbar spine were collected. The X-ray tube was positioned 150 cm away from the examination table, and the X-ray parameters were set at 75 kV and 16 mAs. All radiographic evaluations and subsequent data analyses were performed by independent investigators who were blinded to the group allocation.

Sample collection. At the designated endpoints, rats were euthanized by inhalation of 5-8% isoflurane (1-2 l/min) to induce deep anesthesia. After loss of consciousness, the isoflurane concentration was maintained at 3-5% until spontaneous breathing ceased, and ventilation was continued for an additional 2 min to ensure brain death (no heartbeat, fixed and dilated pupils and the irreversible loss of pedal withdrawal and corneal reflexes). The original surgical incision on the lumbar back was reopened, and the paravertebral muscles on both sides of the spine were dissected to gradually remove the titanium alloy anchor screws and NT springs. Following this, the lumbar spine was resected along the superior margin of L1 vertebra and the inferior margin of L6 vertebra. During the surgical dissection and stripping process, care was taken to protect the bony structure, intervertebral disc tissue and facet joints of the spinal specimens. Normal saline was sprayed continuously to keep the soft tissues moist. Saline-soaked gauze was used to protect the paravertebral muscle tissue specimens and lumbar specimens for subsequent observation.

Micro-computed tomography (micro-CT). The L1-L6 spinal specimens of rats were harvested, and the surrounding soft tissues were removed while preserving the bony structures, intervertebral discs and facet joints. The specimens were scanned using a micro-CT system (Skyscan 1076, SkyScan), ensuring that the scanning plane was parallel to the endplate plane at the apical portion of the convex side of the lumbar vertebrae. The micro-CT scanning parameters were set as follows: Voltage at 70 kV, current at 141 μA, pixel size of 9.485 μm, a rotational scanning range of 180.0˚ and an angular increment of 0.4˚. The spinal specimens were then immersed in a 10% formic acid solution at 4˚C for 48 h for fixation, in preparation for the next experimental steps. After scanning, the micro-CT images of the spinal specimens were imported into the NRecon reconstruction software (version 1.7; Bruker Corporation) to obtain cross-sectional images of the L1-L6 vertebrae of the rat spinal specimens. Since the degeneration between the vertebrae above and below the apical vertebra of the scoliosis is relatively pronounced, the reconstructed image of the lower endplate of the L3 vertebra, located at the apex of the spinal scoliosis, was selected for study.

The cross-sectional images of the lower endplate of the L3 vertebra were imported into the Mimics software (version 19.0; Mimics Medical). An appropriate bone gray scale was selected to reconstruct a 3D image of the endplate and adjacent vertebral bone. Different scanning levels of the bony endplate region were selected as regions of interest (ROI). To reconstruct the pore structure of the endplate, the bony portion of the region was selectively deleted and a 3D model of the remaining pore structure within the endplate was then reconstructed. This resulted in a 3D reconstruction of the pores within the endplate. Using CTAn software (version 1.17.7.2; Bruker Corporation), the trabecular morphometric parameters of the lower endplate of the L3 vertebra were calculated, including bone volume fraction (BV/TV), structure model index (SMI), trabecular bone thickness (Tb.Th), trabecular number (Tb.N), trabecular separation (Tb.Sp), bone mineral density (BMD) and tissue mineral density (TMD).

Transmission electron microscopy (TEM). A total of 3 spinal tissue samples from each group were randomly selected for examination under a TEM. Prior to observation, the samples underwent pre-fixation with 2.5% glutaraldehyde overnight at 4˚C, followed by post-fixation with 1% osmium tetroxide for 1-2 h at room temperature. After dehydration in a graded acetone series (30, 50, 70, 80, 90, 95 and 100%, 10-20 min each step at room temperature), the samples were infiltrated with a blend of dehydrating agent and Epon-812 embedding medium in ratios of 3:1, 1:1 and 1:3 (each for 1-2 h at room temperature), followed by pure Epon-812 resin overnight at room temperature. Light microscope observation of semi-thin sections helped identify ROI, specifically the spinal cord and adjacent areas of the rat spine. Ultra-thin sections, ranging from 60-90 nm in thickness, were then sliced using an ultra-microtome and placed on copper grids. These sections were stained with uranyl acetate for 10-15 min and lead citrate for 1-2 min at ambient temperature. Imaging was carried out using a JEM-1400FLASH transmission electron microscope (JEOL, Ltd.). Quantitative analysis of myelin was conducted on myelin with tight and loose myelin lamellar arrangements. All measurements and g-ratio calculations were performed using ImageJ software (version 1.53t, National Institutes of Health). The g-ratio was defined as the inner diameter of the myelinated fiber divided by the outer diameter of the myelinated fiber.

Hematoxylin and eosin (H&E) and safranin-O-fast green staining. The L4/5 intervertebral disc tissue sections from rats underwent dehydration and paraffin embedding. Subsequently, they were sliced into 5 μm sections. For H&E staining, sections were stained with hematoxylin for 5-10 min, followed by eosin staining for 3 min at room temperature. For safranin-O-fast green staining, sections were stained with Weigert's staining solution for 3-5 min, followed by fast green staining solution for 5 min and safranin staining solution for 5 min at room temperature. The tissue sections then underwent gradient alcohol dehydration, clearing agent treatment for transparency and sealing with neutral balsam. A microscopic camera system (BA210Digital; Motic Industrial Group Co., Ltd.) was used to capture images of the sections, acquiring 100x and 400x microscopic images. Pathological changes in the intervertebral

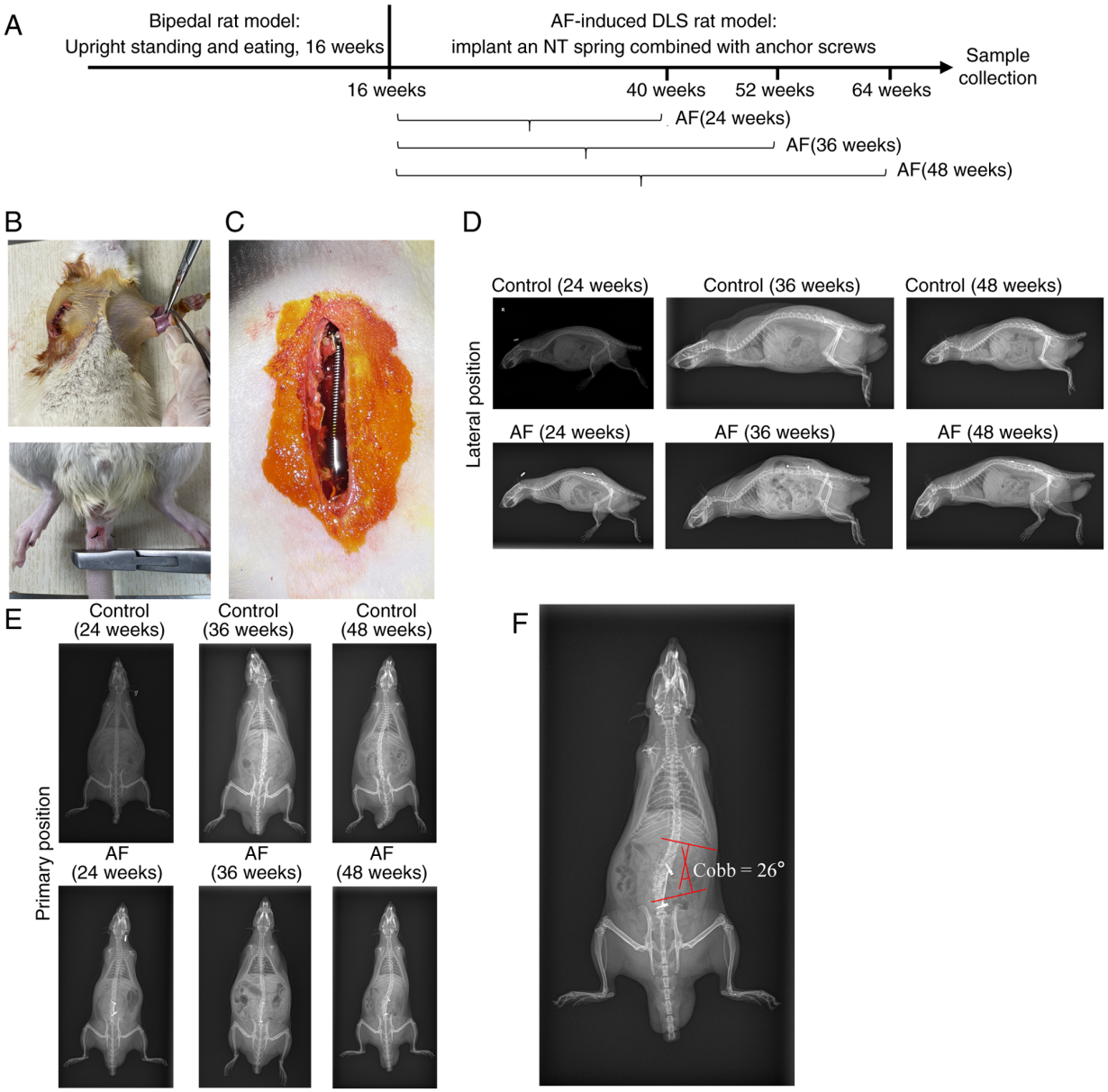

Figure 1. Progress in the model of degenerative lumbar scoliosis in bipedal upright rats. (A) Schematic representation of the experimental timeline. (B) Images of rats with their humerus and tail removed. (C) Pictures of NT springs and anchor screws implanted in rats of the AF group. (D) X-ray examination in the lateral position. (E) X-ray examination in the primary position. (F) The Cobb angle is used to assess the severity of spinal curvature. AF, asymmetric force; w, weeks; NT, nickel-titanium; DLS, degenerative lumbar scoliosis.

disc tissue were analyzed based on pathological features such as chondrocyte degeneration and necrosis, chondrocyte hyperplasia, disordered arrangement of the annulus fibrosus and a decrease in nucleus pulposus cells. A 4-level lesion grading method was adopted, recorded as normal (0 point), mild (1 point, lesion proportion 0-10%), slight (2 points, lesion proportion 11-20%), moderate (3 points, lesion proportion 21-40%) and severe (4 points, lesion proportion 41-100%). In addition, the number of chondrocytes was counted.

Data analysis. The statistical analysis was conducted using SPSS 25.0 software (IBM Corp.). The data were presented as mean ± SD from three independent experiments (n=3). To explore the effect of feeding duration and AF on the DLS model, a two-way ANOVA was utilized, followed by a Bonferroni post-hoc test for multiple comparisons. Data that did not follow a normal distribution were analyzed with the use of Kruskal-Wallis analysis and post hoc Dunn's test, and data are presented as medians and interquartile ranges. Pearson's correlation coefficient was used to assess the association between the Cobb angle and g-ratio. $P<0.05$ was considered a statistically significant difference.

Results

Progress in the DLS bipedal upright rat model. Rats underwent surgical procedures to amputate their humerus and tails to establish a bipedal model (Fig. 1A). As the rats grew, the food and water in their cages were continuously raised to encourage them to maintain a standing and walking posture. Rats in the AF group were implanted with NT springs and anchor screws and were housed separately for 24, 36 and 48 weeks to establish

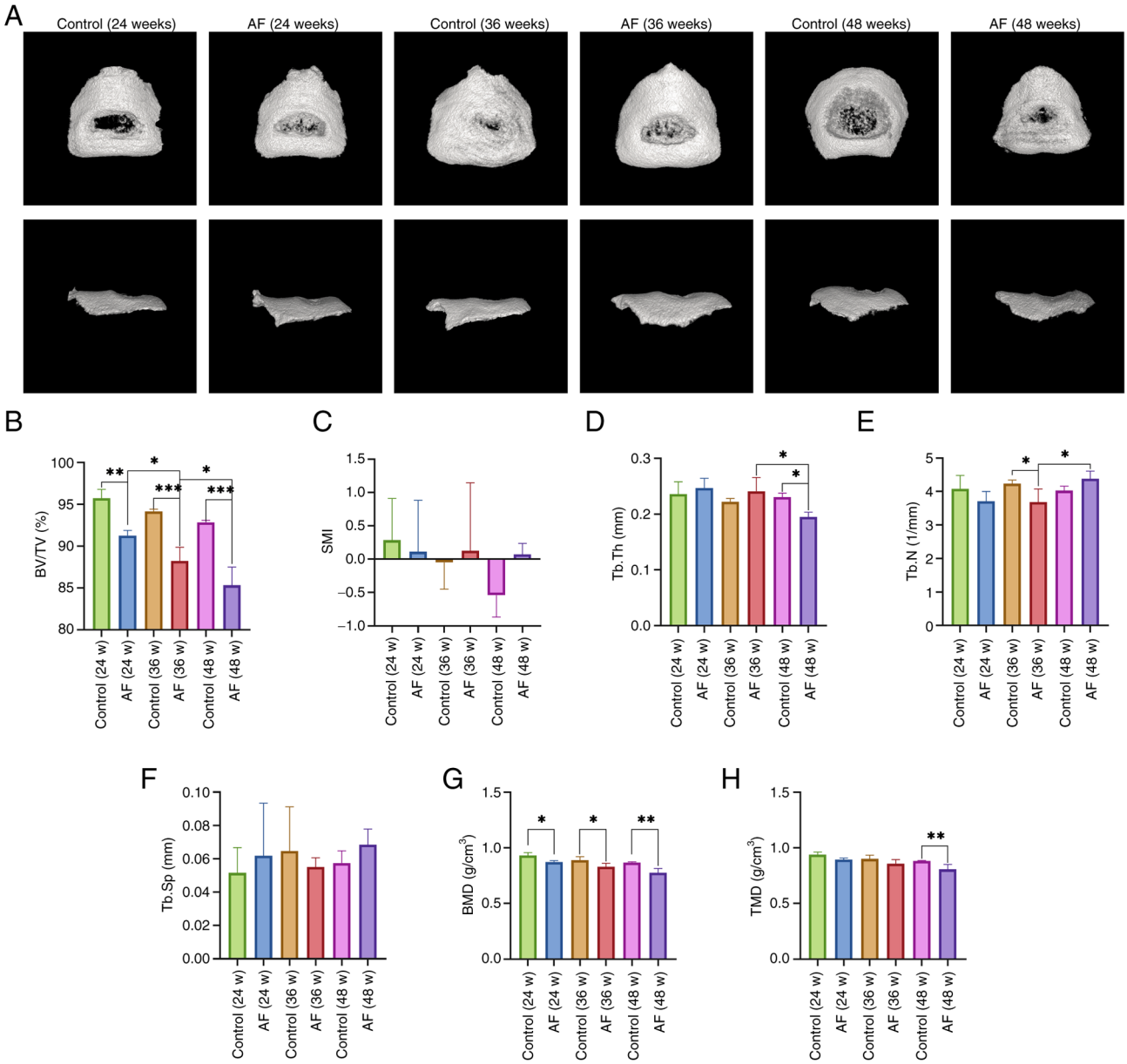

Figure 2. Micro-CT images and micro-architecture parameters of L1-L6 spinal specimens. (A) Micro-CT 3D images in all groups. (B) Micro-CT analyses of bone volume fraction in each group. (C) Micro-CT analyses of SMI in each group. (D) Micro-CT analyses of Tb.Th in each group. (E) Micro-CT analyses of Tb.N in each group. (F) Micro-CT analyses of Tb.Sp in each group. (G) Micro-CT analyses of BMD in each group. (H) Micro-CT analyses of TMD in each group. Multiple comparisons were performed using two-way ANOVA with Bonferroni post hoc test, and the data were presented as mean ± SD (n=3). *P<0.05, **P<0.01 and ***P<0.001. AF, asymmetric force; w, weeks; micro-CT, micro-computed tomography; BV/TV, Tb.Th, trabecular bone thickness; Tb.N, trabecular number; SMI, structure model index; Tb.Sp, trabecular separation; TMD, tissue mineral density; BMD, bone mineral density.

a DLS model (Fig. 1B and C). X-ray examination of the rats' spines in primary position and lateral position (Fig. 1D and E) revealed that no scoliosis occurred in the lumbar vertebrae of the control bipedal rats at 24, 36 and 48 weeks. However, rats in the AF group displayed more pronounced scoliosis in their lumbar vertebrae over time, with structural scoliosis forming at 48 weeks, with the Cobb angle=26˚ (Fig. 1F), indicating the successful establishment of a DLS bipedal rat model.

Changes of the micro-pore structure of the lumbar endplate in the DLS bipedal rat model. Using Mimics software, the vertebral endplate bone was reconstructed to obtain a 3D image, and the canal structure within the vertebral endplate was also reconstructed to generate a 3D model (Fig. 2A). As shown in Fig. 2B, the BV/TV indices for the AF (24 weeks), AF (36 weeks) and AF (48 weeks) groups were 91.28±0.61%, 88.23±1.64% and 85.33±2.18%, respectively. Compared with the control groups at each corresponding time point, the BV/TV index of the L3 lower vertebral endplate in the AF groups decreased significantly in a time-dependent manner (both P<0.05), indicating that AF may contribute to a reduction in lumbar bone volume, suggesting changes in bone structure and bone mass. Fig. 2C demonstrated no significant difference in SMI, implying that AF had no notable effect on trabecular spacing and skeletal muscle index. As illustrated in Fig. 2D, the Tb.Th index was significantly lower in the AF (48 weeks) group compared with the control (48 weeks) group (P<0.05), indicating that AF may have caused trabecular thinning and

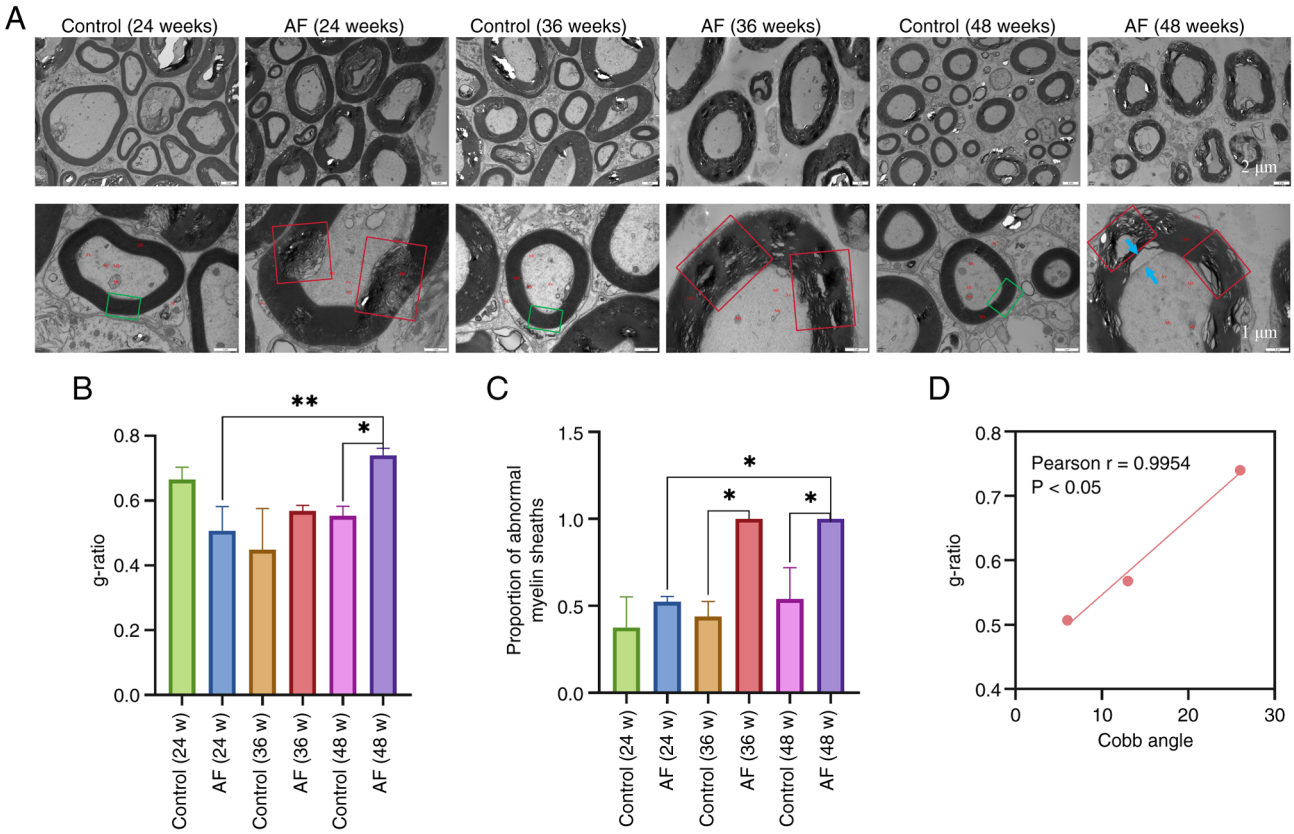

Figure 3. The evaluation of the ultrastructure of spinal cord nerve fibers under transmission electron microscope. (A) Representative images of the spinal tissue samples (top row scale bar, 1 μm; bottom row scale bar 2 μm). The green box indicates that the myelin lamellae are closely arranged, and the red box indicates that the myelin lamellae are loosely arranged and dissolved. Blue arrows indicate demyelination. (B) The g-ratio of myelin. (C) Proportion of abnormal myelin sheaths. (D) Pearson's correlation analysis between the Cobb angle and g-ratio. Multiple comparisons were performed using two-way ANOVA with Bonferroni post hoc test, and the data were presented as mean ± SD (n=3). *P<0.05 and **P<0.01. AF, asymmetric force; w, weeks.

reduced bone strength, thereby decreasing the resistance of the bone to bending and compression. Fig. 2E showed a significant decrease in the Tb.N index in the AF (36 weeks) group compared to the control (36 weeks) group (P<0.05). However, there was an increase in the Tb.N index in the AF (48 weeks) group compared with the AF (36 weeks) group (P<0.05). This might be due to enhanced osteoclast activity and accelerated bone resorption leading to trabecular loss in the early stages of AF, while long-term AF may trigger osteoblast activation, resulting in increased new bone formation and the development of new trabecular branches. Fig. 2F revealed a trend of increasing Tb.Sp index in the AF (48 weeks) group, although the difference was not statistically significant, suggesting that AF may have some impact on the overall porosity of trabecular bone. As presented in Fig. 2G, the BMD index of the L3 lower vertebral endplate was significantly reduced in the AF groups compared with the control groups at each corresponding time point (P<0.05, P<0.01). This suggested that AF was associated with bone loss in the L3 lower vertebral endplate, marked microstructural damage to trabecular bone, which may alter spinal stress distribution and induce scoliosis. Lastly, Fig. 2H demonstrated a significant decrease in the TMD index in the AF (48 weeks) group compared with the control (48 weeks) group (P<0.01), indicating that AF may reduce the mineral content and distribution density in the bone matrix of intervertebral disc tissue, leading to decreased bone stiffness, reduced resistance to deformation and increased susceptibility to scoliosis. In summary, long-term AF may result in bone loss, deterioration of bone structure, decreased bone strength and the development of DLS by reducing BV/TV, Tb.N, BMD, TMD and Tb.Th in the L3 lower vertebral endplate.

Ultrastructural changes of spinal myeloid nerve fibers in the DLS bipedal rat model. The ultrastructure of spinal cord nerve fibers was examined using an electron microscope. Fig. 3A illustrates that in the control groups at 24, 36 and 48 weeks, the medullary nerve fibers appeared normal. Specifically, the mitochondrial structure within the axons was unremarkable, exhibiting a clear cristae structure and uniform matrix electron density. Additionally, microfilaments and microtubules were discernible. The myelin lamina exhibited a compact arrangement, and the myelin sheath was encircled by Schwann cells. However, at 48 weeks of AF treatment, notable abnormalities in the medullary nerve fibers were detected in the AF group. These abnormalities included demyelination, a loosely arranged and dissolved myelin lamina. Although the myelin sheath was still surrounded by Schwann cells, the observed damage progressed with time in this group. In summary, within the context of an aging DLS bipedal rat model, prolonged asymmetric stress may result in structural damage to the medullary nerve fibers, with the severity of damage escalating over time. The continuous wrapping of the myelin sheath by Schwann cells may

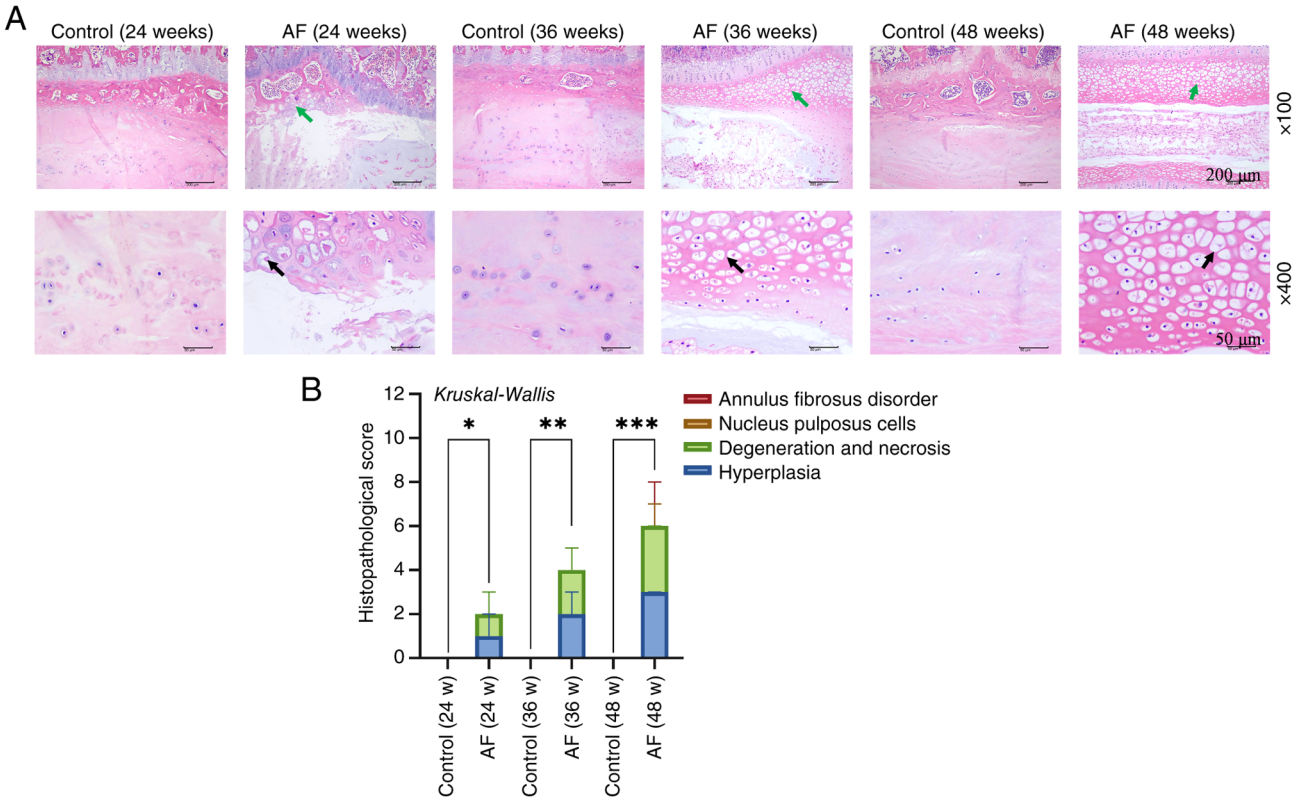

Figure 4. Long-term AF aggravates intervertebral disc damage in the degenerative lumbar scoliosis bipedal rat model. (A) H&E staining of L4/5 intervertebral disc tissue. Green arrows indicate chondrocyte proliferation; black arrows indicate degeneration and necrosis of chondrocytes (top scale bar, 50 μm; bottom scale bar 200 μm). (B) Histological score assessment based on H&E staining. Data were analyzed with Kruskal-Wallis and post hoc Dunn's test, and data are presented as medians and interquartile ranges (n=3). *P<0.05, **P<0.01 and ***P<0.001. AF, asymmetric force; w, weeks.

contribute to the pathological repair process. Quantitative results showed that the g-ratio gradually increased over time at 24, 36 and 48 weeks after AF treatment, with a statistically significant difference observed at 48 weeks (P<0.05). The g-ratio at 48 weeks after AF induction was significantly higher than that at 24 weeks (P<0.01; Fig. 3B). The proportion of abnormal myelin (loosely arranged myelin lamellae) was significantly elevated at 36 and 48 weeks after AF treatment, and the value at 48 weeks was markedly higher than that at 24 weeks (P<0.05; Fig. 3C). To further explore the relationship between spinal deformity and neural damage, individual animal data from all AF groups (24, 36 and 48 weeks) was pooled and a Pearson's correlation analysis was performed between the Cobb angle and g-ratio. A significant positive correlation was found (r=0.9954; P<0.05; Fig. 3D), indicating that greater scoliotic curvature was associated with more pronounced demyelination of spinal nerve fibers. This correlation analysis supports the mechanistic link between the severity of the AF-induced structural deformity and the extent of myelinated fiber pathology. These results indicate that AF was associated with thinning and structural loosening of the myelin sheath, thereby increasing the g-ratio.

Long-term AF aggravates the pathological damage of intervertebral disc in the DLS bipedal rat model. The results of H&E staining (Fig. 4A) of the intervertebral disc tissue revealed that in the control group, the nucleus pulposus, annulus fibrosus and cartilage endplate were clearly visible, with a distinct structure of the cartilage endplate. However, in the AF group, chondrocytes surrounding the cartilage endplate exhibited various degrees of degeneration, necrosis and proliferation, along with nuclear pyknosis, fragmentation, cytoplasmic lysis and increased vacuole formation. Additionally, the annulus fibrosus appeared disorganized, and there was a reduction in nucleus pulposus cells. Furthermore, the pathological score of intervertebral disc tissue in the AF group progressed over time, with significant differences observed between AF groups compared with their respective control group (P<0.05, P<0.01, P<0.001; Fig. 4B). In summary, in the aging bipedal rat model of DLS, long-term AF caused degeneration and necrosis of intervertebral disc cartilage endplate cells, disorder of annulus fibrosus and reduction of nucleus pulposus cells and the pathological damage was aggravated with time.

Long-term AF is associated with lumbar chondrocytes proliferation in the DLS bipedal rat model. Safranin-O-fast green staining revealed a significant increase in the number of chondrocytes in the intervertebral disc after 24, 36 and 48 weeks of AF stimulation compared with the control group (P<0.01, P<0.001; Fig. 5A and B). Notably, while the chondrocyte count remained higher in the AF 36-week and AF 48-week groups compared with controls, no significant difference was observed between these two groups. This suggests that long-term AF stimulation may induce compensatory chondrocyte proliferation, contributing to early pathological

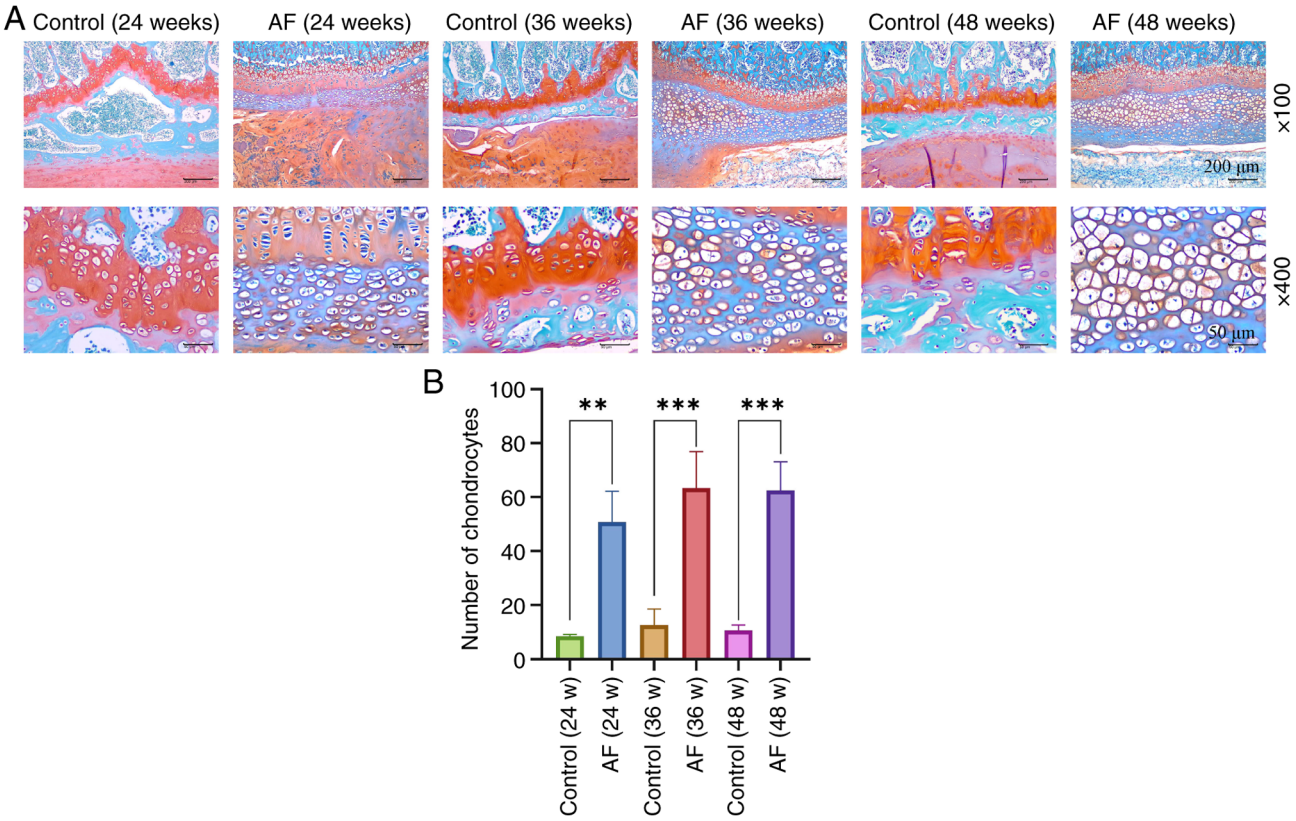

Figure 5. Long-term AF was associated with lumbar chondrocytes proliferation in the degenerative lumbar scoliosis bipedal rat model. (A) Safranin-O-fast green staining of cartilage endplate (top row scale bar, 50 μm; bottom row scale bar, 200 μm). (B) Number of chondrocytes. Multiple comparisons were performed using two-way ANOVA with Bonferroni post hoc test, and the data were presented as mean ± SD (n=3). **P<0.01 and ***P<0.001. AF, asymmetric force; w, weeks.

repair processes, but appear to reach a saturation point with extended exposure.

Discussion

In China, the aging population trend has been accompanied by a growing prevalence of DLS in the elderly (6). Biomechanical factors have gained recognition as key contributors to the pathogenesis of orthopedic disorders (33). In the present study, an AF-induced DLS model was successfully established in aged bipedal rats. The results demonstrated that prolonged AF was associated with progressive spinal deformity by disrupting the bone microstructure of lumbar endplates, inducing spinal nerve demyelination, exacerbating IDD and triggering compensatory chondrocyte hyperplasia, possibly as an early repair attempt. These findings advance the understanding of scoliosis pathogenesis.

The objective of the present study on the DLS animal model is to simulate the onset and progression of human DLS. Such models are essential for elucidating disease mechanisms and evaluating potential interventions. Spinal disorders are closely associated with human upright posture, yet conventional quadrupedal animal models fail to replicate the biomechanical characteristics of the human erect stance. To address this limitation, the present study developed a forced bipedal standing model by amputating the forelimbs and tail, thereby subjecting the spine to vertical loading conditions approximating those in humans. For the bipedal model establishment, 4-week-old rats were selected. Following a 16-week adaptation period, the rats reached skeletal maturity, notably shortening the modeling cycle compared traditional approaches. A progressive feeding height adjustment strategy was implemented to facilitate a behavioral transition from passive adaptation to active maintenance of an upright posture, aligning with the natural progression of human DLS. The use of bipedal rats substantially alleviates the scarcity of upright posture models in spinal research. Furthermore, the present study employed a NT spring to induce scoliosis in rats, enabling the quantification of AF and the application of controlled chronic stress. The device applied unilateral continuous tensile force (12 mm NT spring) to the L1-L6 vertebrae, simulating the mechanical stress environment of human spinal scoliosis and inducing progressive deformity. By extending the observation period to 48 weeks, the present study successfully replicated the chronic progression characteristic of DLS in an animal model for the first time. Additionally, the dual effects of aging and the AF on DLS pathogenesis were investigated.

Numerous animal models have been developed for scoliosis research, encompassing categories such as neuroendocrine (pinealectomy in bipedal rats) (34), mechanical restraint (plaster casting or spinal tethering) (35), gene mutation and neuromuscular injury (36,37). However, these models predominantly focus on idiopathic or congenital scoliosis, and are associated with limitations such as the necessity for continuous external intervention, non-physiological biomechanical environments or an inability to simulate

degenerative changes. Posterior spinal tethering or fusion in mice and rats can induce rapid structural curvature, yet these models fail to replicate the chronic nature and upright loading characteristic of human DLS. Rabbit models of intervertebral disc puncture or compression effectively reproduce disc degeneration but rarely yield consistent coronal plane deformities (26). Large quadrupedal models, such as pigs or non-human primates, more closely approximate human spinal anatomy; however, their application is constrained by high costs and ethical considerations (38). Compared with existing animal models of scoliosis, the AF-induced bipedal DLS model in the present study was established by combining the axial loading of bipedal upright posture with an implantable asymmetric stretch device in the lumbar spine and simulating the chronic aging process. The selection of this bipedal rat model was motivated by the specific scientific question of whether chronic, localized asymmetric mechanical stress under upright axial loading can independently induce and drive the progression of disc degeneration, rather than a claim of absolute anatomical superiority. While porcine or non-human primate models offer closer structural resemblance to human spines, their quadrupedal locomotion fundamentally alters spinal loading patterns. The bipedal rat model uniquely enables the study of chronic, upright axial loading combined with precisely controlled asymmetric force application over a long period (up to 48 weeks), which closely mirrors the decades-long progression in humans. The age-matched control groups controlled for natural aging-related changes, allowing the observed pathologies to be attributed specifically to chronic AF loading. This design prioritizes the replication of functional biomechanical stress and its chronic biological consequences, which is key for mechanistic investigation.

DLS development strongly associated with asymmetric IDD. A study suggests that asymmetric disc degeneration contributes to the pathogenesis of degenerative scoliosis. The intervertebral disc comprises the nucleus pulposus, annulus fibrosus and superior/inferior cartilaginous endplates (39). Previous research has demonstrated that vertebral endplates serve as the primary nutrient source for intervertebral discs (40). In the present study, micro-CT-based three-dimensional reconstruction of endplate structures revealed morphological alterations following 48 weeks of asymmetric loading. In the AF group, the BV/TV index of the L3 inferior endplate exhibited progressive reduction with prolonged intervention duration, indicating time-dependent bone loss. Research has established positive associations between scoliotic curvature and both lumbar index/degree of degeneration, while demonstrating an inverse relationship with BMD (16). The present findings further demonstrated that AF induction significantly decreased Tb.Th, BMD and TMD. These observations suggest that asymmetric mechanical loading influences bone remodeling, ultimately leading to reduced bone density and strength. A significant decrease in BV/TV and BMD, accompanied by non-significant changes in SMI and Tb.Sp (trabecular separation), suggests that the trabeculae in the endplate region are predominantly vertically oriented plate-like structures. This indicates that the primary pathological alteration induced by AF is the widespread thinning of lamellar trabeculae. Furthermore, the trabecular network in this region is dense and well connected. In the early stages of bone loss, the stability of Tb.Sp and the SMI may be maintained through compensatory thickening of the remaining trabeculae, demonstrating a degree of structural resilience. Regarding the consistency of the ROI, the inferior endplate of the L3 vertebral body located within the apical vertebral region of the scoliotic curve was strictly selected. However, it should be acknowledged that the inferior endplate ROI may partially include subchondral cortical bone. This cortical component may mask subtle changes in the underlying trabecular architecture.

The present study untangles the involvement of AF in both vertebral body deformation and cartilaginous endplate damage during scoliosis progression. Histological analysis revealed that asymmetric loading promoted chondrocyte degeneration, chondrocyte hyperplasia, annulus fibrosus disorganization and nucleus pulposus cell reduction within cartilaginous endplates. Chondrocyte degeneration may stem from mechanical stress-induced metabolic disorders, such as mitochondrial dysfunction or elevated oxidative stress (41,42). Secondly, AF may disrupt the lamellar architecture of the annulus fibrosus, causing collagen fiber rupture and consequently compromising disc biomechanical stability. This phenomenon may be associated with upregulated matrix metalloproteinase expression, leading to collagen degradation (43). Furthermore, mechanical stress-induced nucleus pulposus cell reduction is likely associated with enhanced apoptosis (44). As these cells synthesize proteoglycans, their depletion diminishes disc water retention capacity, exacerbating degenerative processes (45). Additionally, lumbar scoliosis may induce segmental instability, resulting in vertebral lateral slippage and rotation that mechanically stretches nerve roots (46). Chronic traction subjects intraneural myelinated fibers to excessive mechanical stress, causing fiber damage/rupture and impaired neural conduction (47,48). The present study suggests that prolonged AF is capable of inducing spinal nerve fiber damage in DLS rat models.

Studies have demonstrated that moderate mechanical stress can regulate the normal maintenance of chondrocytes, thereby promoting proliferation and extracellular matrix (ECM) synthesis. However, excessive stress may trigger chondrocyte apoptosis and inflammatory responses (49,50). In the present study, safranin-O-fast green staining revealed an increase in chondrocytes in the lumbar intervertebral disc tissue sections of AF-induced DLS rats at 24 and 36 weeks. This suggests that during the early stages of AF-induced DLS, chondrocyte proliferation may partially counteract stress-induced damage by synthesizing ECM and enhancing intervertebral disc (IVD) stability. However, no significant difference was observed between 48 and 36 weeks, indicating that prolonged chondrocyte proliferation may lead to alterations in cellular phenotype, reduced ECM synthesis quality and further deterioration of IVD biomechanical properties, thereby exacerbating IDD. Therefore, the dynamic changes in chondrocyte proliferation could serve as a potential biomarker for the early diagnosis of DLS.

However, the present model still has certain limitations. The small IVDs of SD rats complicate precise measurements of vertebral bodies and discs. Some limitations of this

bipedal rat model should be acknowledged. Forelimb and caudal amputation, although effective in reinforcing chronic upright posture, cannot replicate the gradual postural changes observed with aging in humans. Despite the bipedal adaptation, the rat spine retains anatomical differences from the human spine. The ethical use of invasive surgical modifications was carefully weighed against the scientific necessity of replicating human-like upright biomechanics, and all possible refinements were applied to reduce distress of animals. The present study demonstrated preliminary effects of AF on cartilage endplates in DLS but did not monitor temporal changes in chondrocyte proliferation or ECM synthesis. Further research should clarify how AF modulates matrix remodeling, inflammatory responses, mitochondrial function and nucleus pulposus cell apoptosis. The sample size for the terminal analysis is limited by ethical considerations and the exploratory nature of the multimodal phenotype, and future studies with larger sample sizes for these specific endpoints are needed to fully validate the results.

In conclusion, the present study successfully established a novel AF-induced DLS aging bipedal rat model. Long-term AF was associated with progressive spinal deformity, vertebral endplate bone loss, trabecular structural deterioration, intervertebral disc degeneration and myelinated nerve fiber demyelination. Notably, AF triggered compensatory chondrocyte proliferation, which may represent an early reparative response. These findings suggest a biomechanical link between chronic AF loading and DLS progression, providing a basis for exploring therapeutic strategies targeting mechanical stress intervention in DLS.

Acknowledgements

The authors thank West China Hospital, Sichuan University and Dr Nie Hongfei (Chief Physician of the Pain Department and graduate of the Orthopedics Department of West China Hospital, Sichuan University), for providing the scientifically standardized experimental sites, optimal experimental environment and invaluable technical support.

Funding

This work was supported by the General Project of Chongqing Natural Science Foundation (grant no. cstc2021jcyj-msxmX0922).

Availability of data and materials

The data generated in the present study may be requested from the corresponding author.

Authors' contributions

JP conceived the present study, performed the experiments, designed the methodology and wrote the original draft; DC and XZ performed the experiments and collected the data; ZL, AZ and XW analyzed the data; AZ made the figures; KS conceived the present study, obtained funding, designed the methodology, managed the project and reviewed and edited the manuscript. JP and KS confirm the authenticity of all the raw data. All authors read and approved the final version of the manuscript.

Ethics approval and consent to participate

All procedures were approved by the Experimental Animal Ethics Committee of West China Hospital, Sichuan University (approval no. 20230412009) and were conducted in accordance with the ARRIVE 2.0 guidelines.

Patient consent for publication

Not applicable.

Competing interests

The authors declare that they have no competing interests.

References

1. Zheng J, Cheng B, Cook D and Yang Y: Gender differences in degenerative lumbar scoliosis spine flexibilities. Am J Transl Res 13: 13959-13966, 2021.
2. Jimbo S, Kobayashi T, Aono K, Atsuta Y and Matsuno T: Epidemiology of degenerative lumbar scoliosis: A community-based cohort study. Spine (Phila Pa 1976) 37: 1763-1770, 2012.
3. Zhang Z, Song J, Jia S, Tian Z, Zhang Z, Zheng G, Meng C and Li N: How does the correction in lumbar lordosis affect the spinopelvic realignments in degenerative lumbar scoliosis underwent scoliosis surgery? Eur J Med Res 28: 403, 2023.
4. Schwab F, Dubey A, Gamez L, El Fegoun AB, Hwang K, Pagala M and Farcy JP: Adult scoliosis: Prevalence, SF-36, and nutritional parameters in an elderly volunteer population. Spine (Phila Pa 1976) 30: 1082-1085, 2005.
5. Kotwal S, Pumberger M, Hughes A and Girardi F: Degenerative scoliosis: A review. HSS J 7: 257-264, 2011.
6. Geng Z, Wang J, Liu J and Miao J: Bibliometric analysis of the development, current status, and trends in adult degenerative scoliosis research: A systematic review from 1998 to 2023. J Pain Res 17: 153-169, 2024.
7. Wong E, Altaf F, Oh LJ and Gray RJ: Adult degenerative lumbar scoliosis. Orthopedics 40: e930-e939, 2017.
8. Kim HJ, Suk SI and Chang DG: Thoracic myelopathy caused by thoracic degenerative spondylolisthesis and lumbar scoliosis. J Am Acad Orthop Surg Glob Res Rev 9: e24.00232, 2025.
9. Liu J, Li W, Li C, Di J, Guo J and Wang L: Gender-specific risk factors for asymmetric bone density in adult degenerative lumbar scoliosis: A retrospective cohort analysis. Med Sci Monit 30: e944137, 2024.
10. Shafaq N, Suzuki A, Matsumura A, Terai H, Toyoda H, Yasuda H, Ibrahim M and Nakamura H: Asymmetric degeneration of paravertebral muscles in patients with degenerative lumbar scoliosis. Spine (Phila Pa 1976) 37: 1398-1406, 2012.
11. Ishihara Y, Morishita M, Kanzaki K and Toyone T: Age-related progression of degenerative lumbar kyphoscoliosis: A retrospective study. Spine Surg Relat Res 4: 229-236, 2020.
12. Farshad-Amacker NA, Hughes AP, Aichmair A, Herzog RJ and Farshad M: Determinants of evolution of endplate and disc degeneration in the lumbar spine: A multifactorial perspective. Eur Spine J 23: 1863-1868, 2014.
13. Wang W, Li W and Chen Z: Risk factors for screw loosening in patients with adult degenerative scoliosis: The importance of paraspinal muscle degeneration. J Orthop Surg Res 16: 448, 2021.
14. Smit TH: Adolescent idiopathic scoliosis: The mechanobiology of differential growth. JOR Spine 3: e1115, 2020.
15. Izzo R, Guarnieri G, Guglielmi G and Muto M: Biomechanics of the spine. Part I: Spinal stability. Eur J Radiol 82: 118-126, 2013.
16. Ding WY, Yang DL, Cao LZ, Sun YP, Zhang W, Xu JX, Zhang YZ and Shen Y: Intervertebral disc degeneration and bone density in degenerative lumbar scoliosis: A comparative study between patients with degenerative lumbar scoliosis and patients with lumbar stenosis. Chin Med J (Engl) 124: 3875-3878, 2011.

17. Iorio JA, Jakoi AM and Singla A: Biomechanics of degenerative spinal disorders. Asian Spine J 10: 377-384, 2016.
18. Liu Y, Pan A, Hai Y, Li W, Yin L and Guo R: Asymmetric biomechanical characteristics of the paravertebral muscle in adolescent idiopathic scoliosis. Clin Biomech (Bristol) 65: 81-86, 2019.
19. Wang L, Zhang B, Chen S, Lu X, Li ZY and Guo Q: A validated finite element analysis of facet joint stress in degenerative lumbar scoliosis. World Neurosurg 95: 126-133, 2016.
20. Rustenburg CME, Kingma I, Holewijn RM, Faraj SSA, van der Veen A, Bisschop A, de Kleuver M and Emanuel KS: Biomechanical properties in motion of lumbar spines with degenerative scoliosis. J Biomech 102: 109495, 2020.
21. Li QY, Zhong GB, Liu ZD and Lao LF: Effect of asymmetric tension on biomechanics and metabolism of vertebral epiphyseal plate in a rodent model of scoliosis. Orthop Surg 9: 311-318, 2017.
22. Chen F, Chen S, Jing X, Peng F, Du Y, Li J, Fan Y, Cui Z, Gu G, Zhang H, *et al*: Simulated microgravity-driven mechanical unloading rescues PIEZO1-overexpression-induced growth plate ossification and retards adolescent idiopathic scoliosis. NPJ Microgravity 12: 62, 2026.
23. Mente PL, Aronsson DD, Stokes IA and Iatridis JC: Mechanical modulation of growth for the correction of vertebral wedge deformities. J Orthop Res 17: 518-524, 1999.
24. Guo W, Wang Z, Song M, Yang W, Zhang H, Yang W, Wang S, Ma R and Ge Z: Biomechanical evaluation of oblique lateral interbody fusion with various fixation methods for degenerative lumbar scoliosis: A finite element analysis considering different bone densities. Front Bioeng Biotechnol 13: 1562268, 2025.
25. Wang L, Wang H, Wang X, Ma Z, Tian Y, Yuan S, Feng S and Liu X: Radiographic parameter differences in degenerative scoliosis with/without degenerative lumbar spondylolisthesis. Eur Spine J 34: 2828-2837, 2025.
26. Zhang J, Shu Y, Zhu Q, Zhang Z, Li W, Sha P and Zheng S: Lumbar facet joint degeneration contributes to degenerative lumbar scoliosis induced by asymmetric stress in rabbits. Nan Fang Yi Ke Da Xue Xue Bao 39: 993-997, 2019 (In Chinese).
27. Liu L, Zhu Y, Han X and Wu Y: The creation of scoliosis by scapula-to-contralateral ilium tethering procedure in bipedal rats: A kyphoscoliosis model. Spine (Phila Pa 1976) 36: 1340-1349, 2011.
28. Silva CA, Guirro RRJ, Delfino GB and Arruda EJ: Proposal of non-invasive experimental model to induce scoliosis in rats. Rev Bras Fisioter 16: 254-260, 2012.
29. Zhang H, Wang C, Wang W, Wu Z and Qiu G: Novel experimental scoliosis model in immature rat using nickel-titanium coil spring. Spine (Phila Pa 1976) 38: E1179-E1188, 2013.
30. Percie du Sert N, Hurst V, Ahluwalia A, Alam S, Avey MT, Baker M, Browne WJ, Clark A, Cuthill IC, Dirnagl U, *et al*: The ARRIVE guidelines 2.0: Updated guidelines for reporting animal research. BMC Vet Res 16: 242, 2020.
31. Yang S, Zheng C, Jiang J, Lu F, Xia X, Zhu W, Jin X and Ma X: The value of applying a melatonin antagonist (Luzindole) in improving the success rate of the bipedal rat scoliosis model. BMC Musculoskelet Disord 18: 137, 2017.
32. Yang D, Hu W, Li H, Shao YC, Shan JC, Xiong X and Shuang F: Establishment of a bipedal rat model of lumbar facet joint osteoarthritis using intraarticular injection of urinary plasminogen activator. J Orthop Surg Res 17: 447, 2022.
33. Chiu AP, Chia C, Arendt-Nielsen L and Curatolo M: Lumbar intervertebral disc degeneration in low back pain. Minerva Anestesiol 90: 330-338, 2024.
34. Machida M, Saito M, Dubousset J, Yamada T, Kimura J and Shibasaki K: Pathological mechanism of idiopathic scoliosis: Experimental scoliosis in pinealectomized rats. Eur Spine J 14: 843-848, 2005.
35. Paranjape CS, Upasani VV, Newton PO, Masuda K, Bomar JD, Johnson A and Catanzano AA: Lateral suspension bending casting in the treatment of early-onset scoliosis. J Pediatr Soc North Am 12: 100212, 2025.
36. Djebar M, Anselme I, Pezeron G, Bardet PL, Cantaut-Belarif Y, Eschstruth A, López-Santos D, Le Ribeuz H, Jenett A, Khoury H, *et al*: Astrogliosis and neuroinflammation underlie scoliosis upon cilia dysfunction. Elife 13: RP96831, 2024.
37. Xie H, Li M, Kang Y, Zhang J and Zhao C: Zebrafish: An important model for understanding scoliosis. Cell Mol Life Sci 79: 506, 2022.
38. Gullbrand SE, Malhotra NR, Schaer TP, Zawacki Z, Martin JT, Bendigo JR, Milby AH, Dodge GR, Vresilovic EJ, Elliott DM, *et al*: A large animal model that recapitulates the spectrum of human intervertebral disc degeneration. Osteoarthritis Cartilage 25:146-156, 2017.
39. Ashinsky BG, Gullbrand SE, Wang C, Bonnevie ED, Han L, Mauck RL and Smith HE: Degeneration alters structure-function relationships at multiple length-scales and across interfaces in human intervertebral discs. J Anat 238: 986-998, 2021.
40. Lotz JC, Fields AJ and Liebenberg EC: The role of the vertebral end plate in low back pain. Global Spine J 3: 153-164, 2013.
41. Koike M, Nojiri H, Ozawa Y, Watanabe K, Muramatsu Y, Kaneko H, Morikawa D, Kobayashi K, Saita Y, Sasho T, *et al*: Mechanical overloading causes mitochondrial superoxide and SOD2 imbalance in chondrocytes resulting in cartilage degeneration. Sci Rep 5: 11722, 2015.
42. Zhang J, Hao X, Chi R, Qi J and Xu T: Moderate mechanical stress suppresses the IL-1β-induced chondrocyte apoptosis by regulating mitochondrial dynamics. J Cell Physiol 236: 7504-7515, 2021.
43. Wise CA, Sepich D, Ushiki A, Khanshour AM, Kidane YH, Makki N, Gurnett CA, Gray RS, Rios JJ, Ahituv N and Solnica-Krezel L: The cartilage matrisome in adolescent idiopathic scoliosis. Bone Res 8: 13, 2020.
44. Qin T, Shi M, Zhang C, Wu J, Huang Z, Zhang X, Li S, Wu Y, Han W, Gao B, *et al*: The muscle-intervertebral disc interaction mediated by L-BAIBA modulates extracellular matrix homeostasis and PANoptosis in nucleus pulposus cells. Exp Mol Med 56: 2503-2518, 2024.
45. Liu Y, Gao GM, Yang KY and Nong LM: Construction of tissue-engineered nucleus pulposus by stimulation with periodic mechanical stress and BMP-2. iScience 25: 104405, 2022.
46. Kleimeyer JP, Liu N, Hu SS, Cheng I, Alamin T, Grottkau BE, Kukreja S and Wood KB: The relationship between lumbar lateral listhesis and radiculopathy in adult scoliosis. Spine (Phila Pa 1976) 44: 1003-1009, 2019.
47. Ghatge SB, Shah RP, Surya N, Sankhala S, Unadkat CJ, Khan GM and Modi DB: Ozone disc nucleolysis in cervical intervertebral disc herniation: A nonrandomized prospective analysis in 246 patients. J Craniovertebr Junction Spine 13: 114-120, 2022.
48. Yeoh S, Warner WS, Eli I and Mahan MA: Rapid-stretch injury to peripheral nerves: Comparison of injury models. J Neurosurg 135: 893-903, 2020.
49. Lieberthal J, Sambamurthy N and Scanzello CR: Inflammation in joint injury and post-traumatic osteoarthritis. Osteoarthritis Cartilage 23: 1825-1834, 2015.
50. Hirose N, Okamoto Y, Yanoshita M, Asakawa Y, Sumi C, Takano M, Nishiyama S, Su SC, Mitsuyoshi T, Kunimatsu R, *et al*: Protective effects of cilengitide on inflammation in chondrocytes under excessive mechanical stress. Cell Biol Int 44: 966-974, 2020.